Conductive Polymer Composites: Electrical, Thermal, and Rheological Study of Injected Isotactic Poly(propylene)/ Long Stainless-Steel Fibers for Electromagnetic Interferences Shielding

J. F. Feller,[1] S. Roth,[2] A. Bourmaud[2]

[1]*Laboratory of Polymers, Properties at Interfaces and Composites (L2PIC), South Brittany University, Lorient, France*
[2]*Institut für Allgemeinen Maschinenbau und Kunststofftechnik, Chemnitz University of Technology, Chemnitz, Germany*

Received 23 May 2005; accepted 1 September 2005
DOI 10.1002/app.23141
Published online 00 Month 2005 in Wiley InterScience (www.interscience.wiley.com).

ABSTRACT: The influence of long stainless-steel fibers (LSSF) on electrical, rheological, and calorimetric properties of conductive composites with poly(propylene) matrix was investigated as a function of filler content from $\phi = 0.15$ to 3.6% v/v (1.3 to 23.5% w/w). The results show interesting features of the crystallization process: fibers act as nucleating agents and generate transcrystalline phases in quiescent conditions. LSSF also influences the flow properties and the dynamic rheological behavior, which is evidenced by evolution of G' and G'' curves with filler content. Finally, SEM pictures of injected samples were used to determine the distribution and orientation of the fibers in the part thickness at different distances from the injection point. © 2006 Wiley Periodicals, Inc. J Appl Polym Sci 100: 3280–3287, 2006

Key words: isotactic; polypropylene; electrical conductivity; electromagnetic shielding; rheology; differential scanning calorimetry; long stainless steel fibers

INTRODUCTION

Conductive polymer composites (CPC) obtained by dispersing conductive fillers into a polymer matrix can be used to design housings with electromagnetic shielding capabilities.[1] One of the key points to obtain parts having reproducible electrical properties by injection-molding is the control of the filler dispersion within the matrix. Because of the high shearing during injection under high pressure, the filler is subjected to orientation depending on the geometry of the part and the nature of the melted CPC flow behavior.

Among several conductive fillers available, carbon particles,[2–4] carbon fibers,[5,6] metal particles[7,8] or conducting polymers,[9] long stainless-steel fibers (LSSF)[10] combine the advantages of being less sensitive to orientation than short fibers are, and of leading to a lower percolation threshold than that of particles because of their high length to diameter aspect ratio. Nevertheless, no model exists to describe the orientation of LSSF during injection-molding. Thus, it is necessary to identify and control the different parameters responsible for LSSF dispersion and orientation, as they will govern the final electrical properties of the part.

For a better understanding of the conductive network structure development during the mold filling and part solidification, we have investigated the influence of the LSSF on both rheological and thermal properties of poly(propylene)/LSSF as a function of filler content.

Correspondence to: J. F. Feller (jean-francois.feller@univ-ubs.fr).

Contract grant sponsor: Erasmus Program.

EXPERIMENTAL

Materials

The main characteristics of neat poly(propylene) (PP) used in this study (Novolen 1100N from BASF, Ludwigshafen, Germany) are given in Table I. To obtain the desired electrical conductivity, neat PP was blended with a master batch of PP filled with 50 w/w % LSSF from Ticona (Kelsterbach, Germany) (referenced as Celstran S), allowing to reach a range of LSSF content from $\phi = 1.3$ to 23.5% w/w (0.15 to 3.6% v/v). The steel fibers used in this blend are high quality alloyed V4A (18% chrome, 8–9% nickel, less than 2% manganese, martensite content 88–94%); the fibers have a density of $d = 7.98$ g cm^{-3}, an average length of $L = 10$ mm, and a diameter of $D = 8$ μm leading to a high shape factor of $L/D = 1250$.

TABLE I
Characteristics of the Pristine Poly(propylene)

Electrical surface resistivity	ρ (10^{14} Ω cm)
Melting temperature	T_m = 164.45°C
Nonisothermal crystallization temperature	$T_{n,c}$ = 108.19°C
Glass transition temperature	T_g = −3.07°C
Density	d = 0.95 g cm^{-3}
Tensile strength	σ = 35 MPa
Tensile modulus	E = 1.55 GPa

Techniques

Electrical resistivity was measured using a four probes device designed according to the ISO 3915 norm (cf. Fig. 1). The multimeter used for voltage and current measurement was a Voltcraft VC222 and the generator was a RFT 3214. In Figure 1, index 1 corresponds to current measurement electrode, 2 to sample (CPC), 3 to voltmeter, 4 to voltage measurement electrode, 5 to insulating plate, 6 to insulating support in PVC, and 7 to blades in copper. The standard penetration depth used for the measurement electrodes, 1 mm, was controlled by two lateral wedges.

Isothermal crystallization of PP/LSSF CPC was followed using a Leica DMLP optical microscope, in polarized light, coupled to an image analysis device Lida and a Mettler Toledo FP 90 hot plate.

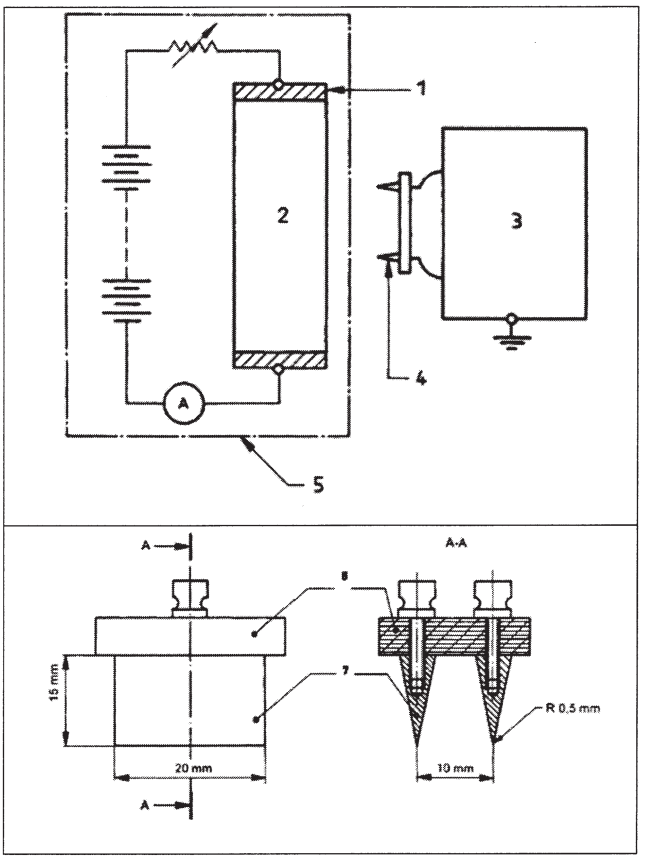

Figure 1 Scheme of ISO 3915 test (up), detail of the electrodes (down).

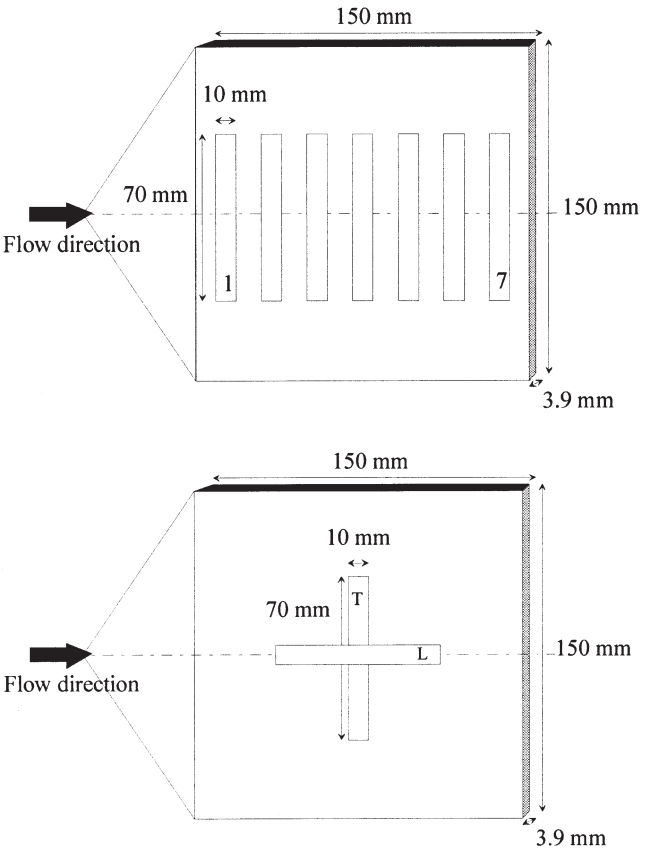

Figure 2 Localization of the samples stamped from the injected plate. Respectively, in the flow direction 1 to 7 (up) and in the longitudinal (L) and transverse (T) direction (down).

Calorimetric measurements were done with a Mettler Toledo DSC 822. The calibration was done with Indium and Zinc. The base line was checked every day. Aluminum pans with holes were used and the sample's mass was ~10 mg. All samples were first heated to 200°C for 5 min to get rid of thermal history. Nonisothermal crystallization and melting temperatures, $T_{c,n}$ and T_m, respectively, were determined from the peak extrema in experiments at ± 10°C min^{-1} heating/cooling rates. To prevent any sample degradation, the experiments were carried out under nitrogen flow. All temperatures measured from a peak extremum (T_c, T_m) are determined at less than ±0.5°C and from a sigmoid (T_g) at less than ±1°C.

Rheological properties of CPC were studied with a Bohlin Gemini rheometer with plate/plate geometry (diameter 20 mm, gap 1.5 mm) in both steady and dynamical modes (γ = 1.5%, after determination of the linear strain range).

Scanning electronic microscopy (SEM) observations were done with a Jeol JSM-6031.

Injection-molding was carried out on a Kraus Maffei KM 90–340 B using the following parameters: melt

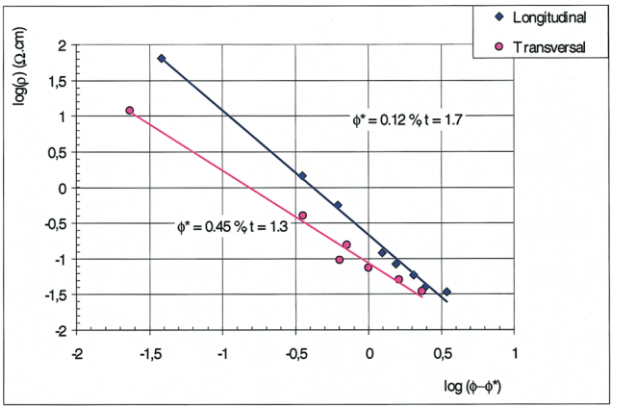

Figure 3 Percolation curves of PP/LSSF CPC in the longitudinal and transverse directions (depth 0.5 mm). [Color figure can be viewed in the online issue, which is available at www.interscience.wiley.com.]

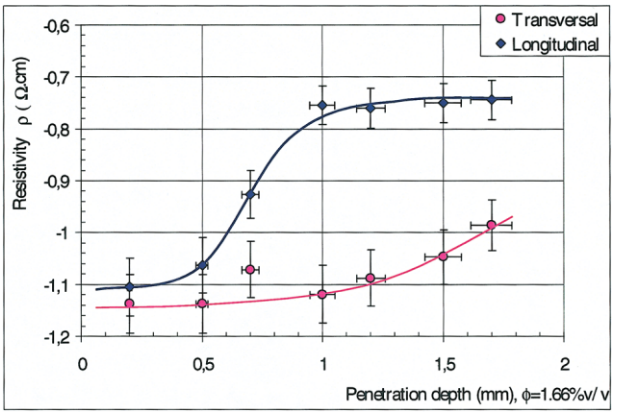

Figure 5 Evolution of resistivity as a function of depth (from 0.2 to 1.7 mm) in transverse and longitudinal direction for PP/1.66% v/v LSSF. [Color figure can be viewed in the online issue, which is available at www.interscience.wiley.com.]

temperature 250°C, mold temperature 30°C, injection time ~1 s. For the following surveys, film-gated test plaques of 150 mm × 150 mm × 3.9 mm were produced.

Sample preparation was done as shown in Figure 2; samples taken from points 1–7 allow following the evolution of properties in flow direction, and samples picked out in directions longitudinal (L) and transverse (T) to flow direction give information on the anisotropy.

RESULTS AND DISCUSSION

Electrical behavior

The first important operation to do when studying CPC is to determine the percolation curve (cf. Fig. 3). This figure shows a phenomenon of conductivity anisotropy which can be quantified determining the percolation parameters ϕ^* and t, respectively, the percolation threshold and the scaling parameter, derived from eq. (1). It can be seen that percolation is achieved for a lower content of LSSF (ϕ^*) in longitudinal direction (0.12% v/v) than that in direction perpendicular to the flow direction (0.45% v/v). These very low values of ϕ^* confirm the interest to use fillers with a very high shape factor, especially for high-density fillers like stainless steel (d = 8). Moreover, the very low values of ϕ^* in both longitudinal and transverse directions show that the orientation process is not sufficient to drastically decrease fibers' connectivity in the part skin.

$$\rho = \rho_0(\phi - \phi^*)^t \quad (1)$$

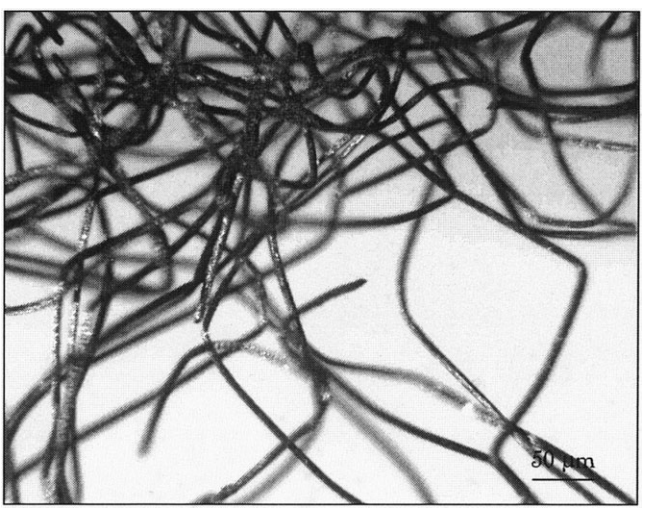

Figure 4 Photo of the LSSF after complete burning of the PP matrix.

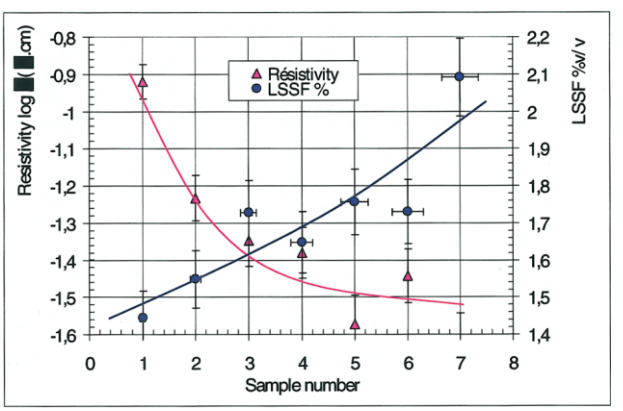

Figure 6 Correlation between resistivity and LSSF content as a function of distance from injection point for PP/1.66% v/v LSSF (depth 0.5 mm). [Color figure can be viewed in the online issue, which is available at www.interscience.wiley.com.]

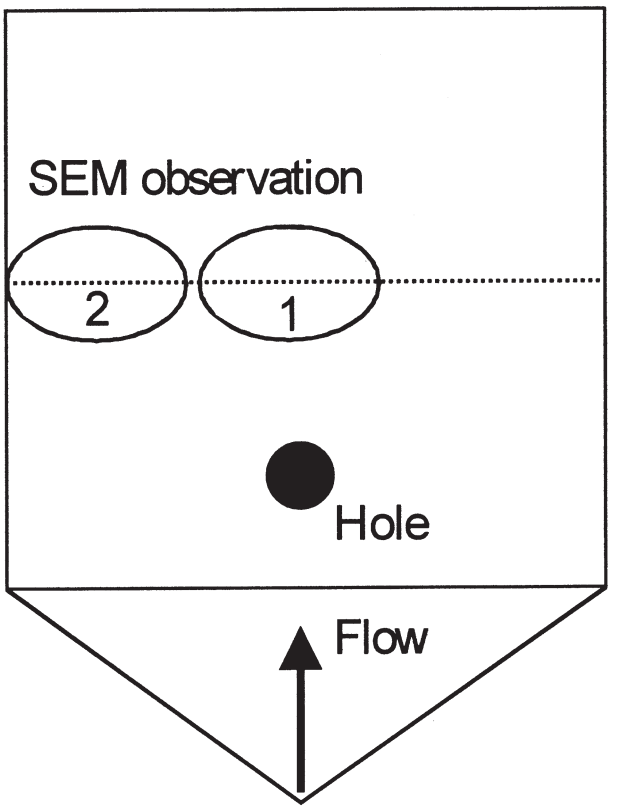

Figure 7 Localization of sites for SEM observation.

where ρ is the resistivity, ρ_0 is a constant, ϕ and ϕ^* are respectively, the filler volume content and the filler content at the percolation threshold, t is the scaling parameter.

Interpretation of "t" values gives additional information concerning the spatial distribution of the fibers. Values of $t = 2$ are theoretically obtained for spheres statistically dispersed in a matrix in three dimensions,[11] whereas $t = 1.1$ means that the fibers are conformed in empty spheres or dispersed within an interface in two dimensions.[12] But in some cases, non universal values of t, much higher than 2, are found with short carbon fibers, for example.[5] For LSSF, the values obtained $t_{\text{longitudinal}} = 1.7$ and $t_{\text{transverse}} = 1.3$, suggest that fibers tend to be organized in 3D and 2D patterns in the longitudinal and transverse directions, respectively. Keeping in mind that these percolation curves have been established at a low distance from the surface (0.5 mm), these results suggest a more important fiber orientation in the flow direction resulting in a lower connectivity between the fibers. As a consequence, in the transverse direction, the resistivity is found to be higher for the same content. This is consistent with an alignment of fibers in the skin during the injection process, which is also observed with short fibers. Thus, in the conditions of our experiments, it is better not to interpret "t" exponent in terms of 3D or 2D distribution but with regard to fiber orientation. With the same kind of material, Bridge et al.[13] have used a model to predict the percolation threshold from the fiber conformation supposed to be perfectly helical. But in fact, as it can be seen in Figure 4, after burning of the PP matrix, the fibers are much entangled and can more likely be assimilated to random coils than to rigid rods or helices. Moreover, fibers are heterogeneously dispersed not only in the surface but also in the thickness of the sample. Figure 5 shows that in the center of the part, position L and T in Figure 2, resistivity increases from the skin to the core and this more quickly in the longitudinal than in the transverse direction.

It is interesting to notice in Figure 6, which shows the evolution of resistivity in the flow direction (samples were cut out according to Fig. 2), that, as the distance from the injection gate increases, resistivity decreases and the correlation of resistivity with fiber content diverges. This means that, on one hand, fibers

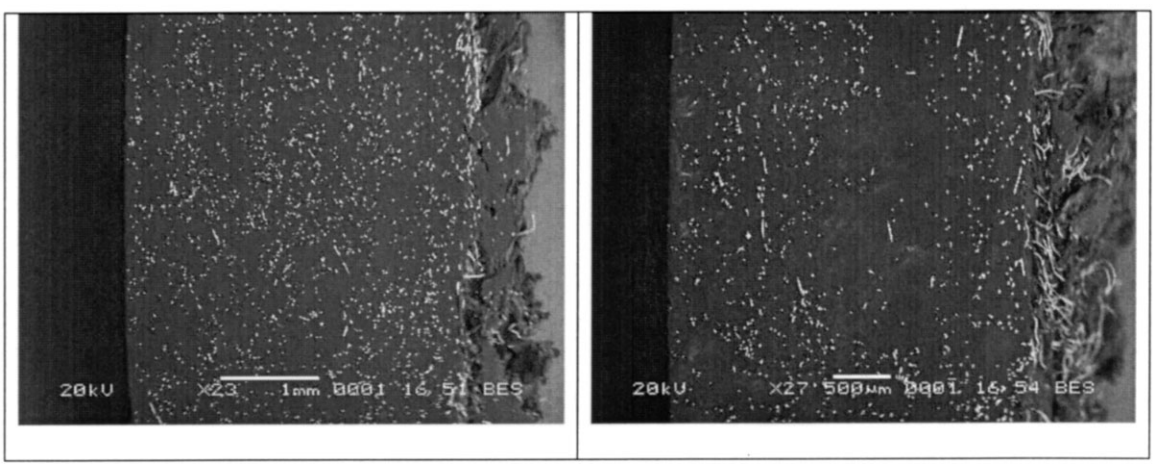

Figure 8 SEM observation of transverse cut in zone 1 and 2 respectively, from right to left.

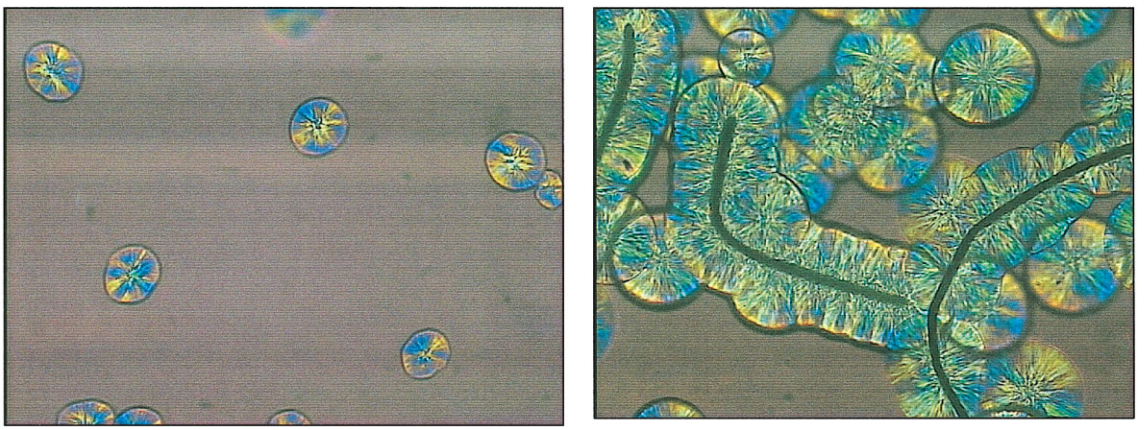

Figure 9 From left to right, spherulites of PP and cylindrites of PP/0.56% v/v LSSF isothermally crystallized at 135°C for 21 min. [Color figure can be viewed in the online issue, which is available at www.interscience.wiley.com.]

are more concentrated in point 7, and on the other hand, at the end of the flow path (point 7), the fibers' dispersion is more heterogeneous.

Scanning electronic microscope observations

To complete the electrical measurements, we made SEM observations in the middle of the part, as shown in Figure 7. In this particular case, we wanted to see if the presence of a flow barrier would generate weld lines.

The pictures of Figure 8 are cuts of the part across the whole thickness and these clearly show that in the axis of the flow behind the flow barrier, the core of the part is less concentrated in fibers than that is far from the flow axis where the distribution is more homogeneous.

These SEM pictures also show that the fibers are mainly orientated in the flow direction and that the effect of the obstacle is to decrease the fiber content in the core of the part.

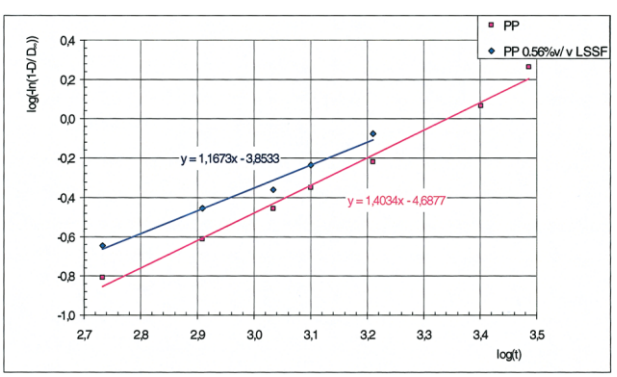

Figure 10 Avrami plots of PP and PP/0.56% v/v LSSF isothermally crystallized at 135°C. [Color figure can be viewed in the online issue, which is available at www.interscience.wiley.com.]

Crystallization

Isothermal crystallization

Optical microscopy isothermal crystallization experiments have been analyzed using the Avrami model[14] presented in eq. (2). Images are obtained regularly to follow the increase of spherulites' diameter D with time for neat and 0.56% v/v LSSF-filled PP (cf. Fig. 9). Pictures are then treated with an image processing software and $\log(-\ln(1 - D_t/D_\infty))$ versus $\log(t)$ curves are subsequently plotted to obtain the graph of Figure 10.

$$\ln\left(1-\frac{D_t}{D_\infty}\right) = -kt^n \qquad (2)$$

where D_t and D_∞ are the spherulites' mean diameter respectively, at time t and at an infinite time, k is the speed constant, and n is the Avrami index.

The comparison of PP and PP/0.56% v/v LSSF crystallization in Figure 9 outlines the differences in size of growing crystalline entities and nucleation type. First, it is very clear from Figure 9 that LSSF give rise to transcrystalline phase in quiescent crystallization conditions. In neat PP, the growth is slower and the nucleation classical. But for PP/0.56% v/v LSSF, the nucleation appears both from classical nuclei and from the fiber's surface.

TABLE II
Crystallization Kinetics Parameters of Isotactic Poly(propylene)

	PP	PP 0.56% (v/v) LSSF
n	1.4	1.17
k	107.8	47.0
G (μm s^{-1})	0.0308	0.034

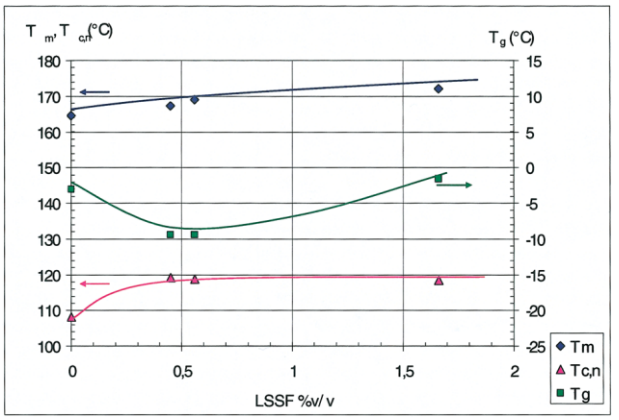

Figure 11 Evolution of phase transition temperatures with LSSF fibers. [Color figure can be viewed in the online issue, which is available at www.interscience.wiley.com.]

The fact that spherulites' diameter is larger in PP/ 0.56% v/v LSSF than in neat PP demonstrates that the presence of fibers influences the crystallization kinetics not only because chains can crystallize from the fiber, but also because they modify the medium properties. In fact, it is likely that LSSF improve thermal conductivity and thus increase heat transfer during crystallization.

Table II shows the kinetics parameters derived from Figure 9 (growth speed G) and Avrami plots of Figure 10 (n Avrami index and k speed constant). The values of n are not very realistic because they suggest an initial nucleation with a 1D/2D growth; despite this, it is clear from Figure 9 that the growth is 2D/3D. Nevertheless, k and G values are more interesting and show that if the global crystallization speed of PP/ 0.56% v/v LSSF is faster (G), the speed constant of PP is more important.

Nonisothermal crystallization

Complementary calorimetric experiments have been done in nonisothermal conditions (constant cooling rate). The evolution of phase transition temperatures with LSSF content are plotted in Figure 11 and theses values together with the enthalpies associated to the transitions are shown in Table III.

Figure 11 shows that $T_{c,n}$, the non isothermal crystallization temperature, increases with LSSF content up to 0.56% v/v at about 10°C (which is significant) and remains constant until 1.66 v/v %. This tendency is consistent with the speed increase already observed in isothermal conditions. The higher $T_{c,n}$ appears the quicker the crystallization.

T_m increases regularly with LSSF content at about 8°C but together with a decrease of about 20% of the melting enthalpy ΔH_m. The fibers speed up crystallization of some chains population but this is to the detriment of crystallinity. This suggests that fibers favor crystallization of chains in thicker lamellae (melting at higher temperature) but that some chains are excluded from these crystals. Future surveys have to show whether this phenomenon could be linked to a viscosity increase unfavorably influencing crystallization.

The evolution of the glass transition temperature is more surprising because a small amount of fibers (less than 0.56 v/v %) leads to a decrease of T_g, whereas amounts over 0.56 v/v % increase T_g to a value superior to that of neat PP for 1.66% v/v LSSF. This first decrease of T_g is important enough (6°C) to justify an explanation. However, for the moment we did not find one. An increase of free volume, or a decrease of intermolecular interaction, which can generally be responsible for a T_g decrease, can hardly be involved herein. In fact, as it will be shown in the following, LSSF tend to increase viscosity instead of plastifying PP chains, which is however consistent with the second part of the curve, the increase of T_g over 0.56% v/v.

Rheological behavior

Steady state mode

Figure 12 shows the flow behavior of the plastic as a function of LSSF content. As neat PP has a Newtonian behavior from 0.001 to 10 s^{-1}, the introduction of a small amount of fibers progressively changes it to pseudoplastic in the whole shear rate range but without completely deleting the transition shear rate at about 10 s^{-1}. This behavior could be linked to mechanical percolation but in our case it is difficult to correlate the value of the threshold obtained to that determined with electrical measurements because of different nature of the samples used in both tech-

TABLE III
Calorimetric Characteristics of Isotactic Poly(propylene) CPC from DSC

Materials	T_m (°C)	T_g (°C)	$T_{c,n}$	ΔH_m (J g^{-1})	ΔH_c (J g^{-1})
PP	164.45	−3.07	108.19	101.99	102.72
PP 0.45% (v/v) LSSF	167.33	−9.43	119.09	−97.22	98.3
PP 0.56% (v/v) LSSF	169.03	−9.41	118.80	−94.53	93.8
PP 1.66% (v/v) LSSF	172.17	−1.66	118.31	−83.64	81.39

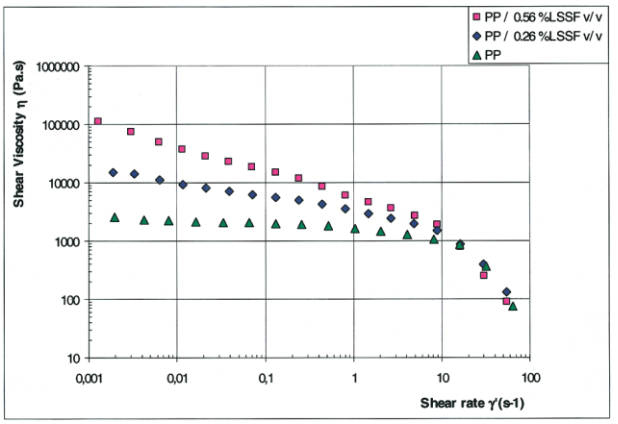

Figure 12 Shear viscosity η in steady mode of CPC at 220°C. [Color figure can be viewed in the online issue, which is available at www.interscience.wiley.com.]

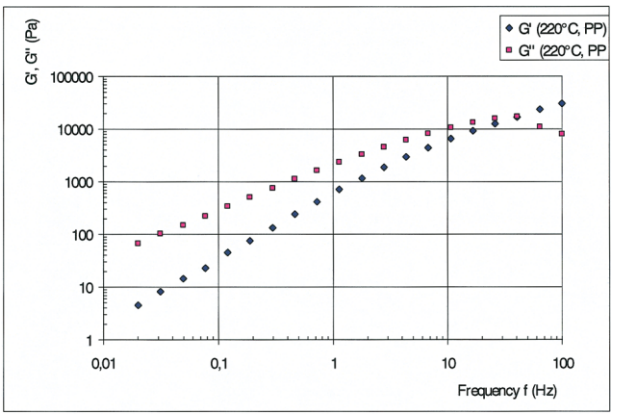

Figure 14 G' and G'' evolution with frequency at 220°C for neat PP. [Color figure can be viewed in the online issue, which is available at www.interscience.wiley.com.]

niques (volume and fiber distribution) even at equivalent fiber content.

Figure 13 evidences the reinforcing effect of fibers on PP flow, especially at low shear rates. The viscosity increase with LSSF content can be fitted with an exponential law except over $\dot{\gamma} > 10s^{-1}$, where the development is linear. This result suggests that fibers do not have many consequences on the flow during the process at high shearing, but at lower shear rate, there are important interactions between fibers and macromolecules.

Dynamic mode

To study the dynamics of the CPC in the melt, we have investigated its behavior, G' and G'' evolution with frequency. Curves obtained for neat PP at 220°C are rather classical (Fig. 14), G' and G'' cross at about 40 Hz and have the expected low frequency slopes at low frequency of 2 and 1, respectively.

If we look now at Figures 15 and 16, we can observe that the crossover is not shifted with LSSF, although. The modulus range of G' and G'' increases progressively by 4 decades, with an increasing fiber content starting from neat PP to PP/0.93% v/v LSSF. This development goes along with a progressing fiber network caused by the increasing filler content that suppresses the initial flow behavior at low frequencies.

It can also be noticed that G', the storage modulus, becomes superior to G'' in the whole frequency range as the fiber content increases.

These modifications of rheological behavior induced by fibers, although not very important at high shear rate or frequency (in the gates), can have a very important impact at a low frequency and low shear rate in thick parts.

CONCLUSIONS

PP/LSSF CPC are used to design injected parts for EMI shielding. Although steel fibers provide very in-

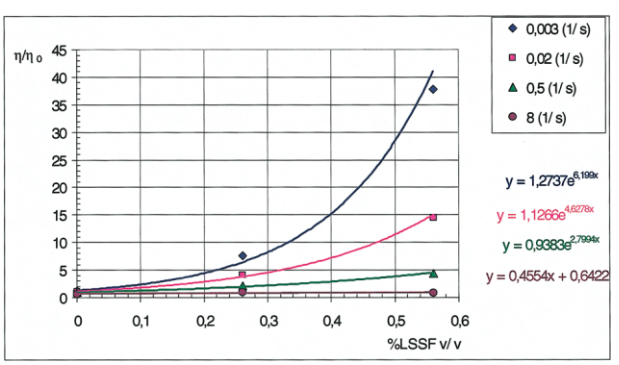

Figure 13 Reinforcing effect evidenced by shear viscosity ratio h/h_0 evolution with LSSF content at 220°C as a function of shear rate. [Color figure can be viewed in the online issue, which is available at www.interscience.wiley.com.]

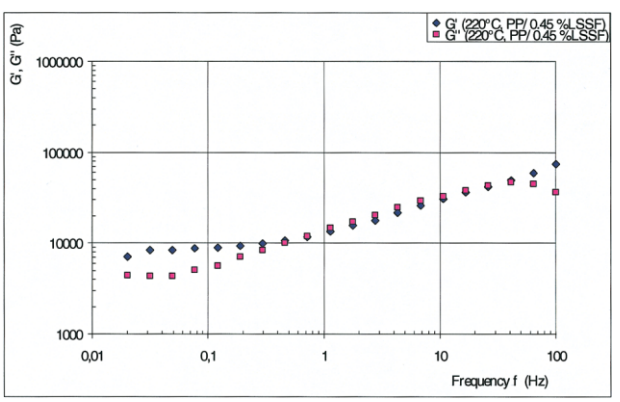

Figure 15 G' and G'' evolution with frequency at 220°C for PP/0.45% v/v LSSF. [Color figure can be viewed in the online issue, which is available at www.interscience.wiley.com.]

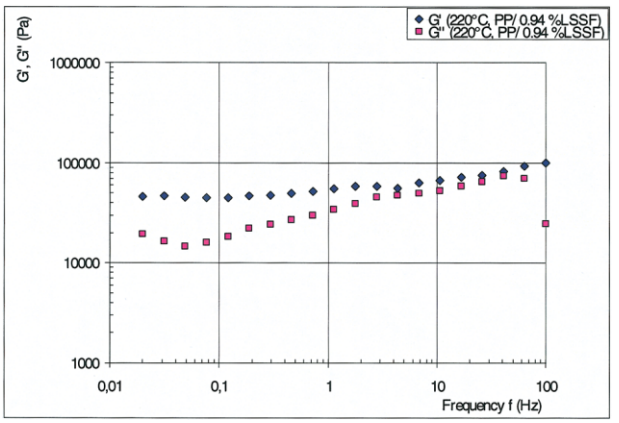

Figure 16 G' and G'' evolution with frequency at 220°C for PP/0.94% v/v LSSF. [Color figure can be viewed in the online issue, which is available at www.interscience.wiley.com.]

teresting electrical properties, i.e., low percolation threshold and high electrical conductivity, they also modify calorimetric and rheological properties leading to a behavior very different from neat PP. T_m and $T_{c,a}$ increase with LSSF content whereas T_g goes through a minimum and ΔH_m decreases. Viscosity increases especially at low shear rates and both G' and G'' increase at low frequency with fiber content that can be explained by the developing steel fiber network with increasing fiber content. As expected from injection-molding process, a heterogeneous dispersion of fibers in the part lead to anisotropic electrical properties, both in flow direction and across the thickness, and electrical measurements were found to be very powerful tools to determine fibers' orientation and dispersion into the matrix. However, this should not influence the application too much, provided that the described phenomena are well controlled.

The authors thank Jérôme Velin, Julien Lucas, and Françoise Peresse for their contribution to this work. Furthermore, we are much obliged to the Ticona AG, Kelsterbach, Germany for providing the steel fiber compound Celstran S for our surveys.

References

1. Roth, S.; Mennig, G. 20th Polym Proc Soc 2004, 49, 1.
2. Breuer, O.; Tzur, A.; Narkis, M.; Siegmann, A. J Appl Polym Sci 1999, 74, 1731.
3. Wu, T. M.; Cheng, J. C. J Appl Polym Sci 2003, 88, 1022.
4. Feller, J. F. J Appl Polym Sci 2004, 91, 2151.
5. Feller, J. F.; Linossier, I.; Grohens, Y. Mater Lett 2002, 57, 64.
6. Zhang, C.; Yi, X. S.; Yui, H.; Asai, S.; Sumita, M. J Appl Polym Sci 1998, 69, 1813.
7. Mamunya, Y. P.; Davydenko, V. V.; Pissis, P.; Lebedev, V. Eur Polym J 2002, 38, 1887.
8. Jia, W.; Tchoudakov, R.; Joseph, R.; Narkis, M.; Siegmann, A. J Appl Polym Sci 2002, 85, 1706.
9. Cho, M. S.; Park, S. Y.; Hwang, J. Y.; Choi, H. J. Mater Sci Eng C 2004, 24, 15.
10. Weber, M.; Kamal, M. R. Polym Compos 1997, 16, 711.
11. Carmona, F. Phys A: Stat Mech Appl 1989, 157, 461.
12. Huang, J. C. Adv Polym Technol 2002, 21, 299.
13. Bridge, B.; Folkes, M. J.; Jahankhani, H. J Mater Sci 1989, 24, 1479.
14. Long, Y.; Shanks, R. A.; Stachurski, Z. H. Prog Polym Sci 1995, 20, 651.